Phys. Status Solidi B **252,** No. 11, 2574–2579 (2015) / **DOI** 10.1002/pssb.201552215

physica status solidi b
www.pss-b.com
basic solid state physics

Epitaxial growth of insulating and superconducting monolayers of $(BETS)_2GaCl_4$ on Ag(111)

Abdou Hassanien[*,1], Biao Zhou[2], Hisashi Tanaka[3], Akira Miyazaki[4], Madoka Tokumoto[3], Akiko Kobayashi[2], Erik Zupanič[1], and Igor Muševič[1,5]

[1] J. Stefan Institute, Jamova 39, 1000 Ljubljana, Slovenia
[2] Nihon University, Sakurajosui, Setagaya-ku, Tokyo 156-8550, Japan
[3] AIST, 1-1-1 Umezono, Tsukuba, Ibaraki 305-8568, Japan
[4] Toyama University, 3190 Gofuku, Toyama shi, Toyama 930-8555, Japan
[5] Faculty of Mathematics and Physics, University of Ljubljana, Jadranska 19, 1000 Ljubljana, Slovenia

Received 16 April 2015, revised 28 August 2015, accepted 16 September 2015
Published online 16 October 2015

Keywords heteroepitaxial growth, Kagome lattice, monolayer superconductors, scanning tunneling microscopy

[*] Corresponding author: e-mail Abdou.Hassanien@ijs.si, Phone: +386 41 2999 56, Fax: +386 1 477 31 91

The ability to fabricate crystalline monolayers of confined superconducting or magnetic condensate on surfaces is a key issue to realize new functionalities and understand the nature of competing orders in their phase diagram at the nanoscale. Herein, we outline a reliable method to pattern a monolayer of superconducting islands and Kagome lattice of $(BETS)_2GaCl_4$ (where BETS = bis(ethylenedithio) tetraselenafulvalene) on Ag(111). At a deposition temperature of 125 K, $(BETS)_2GaCl_4$ dimers form Kagome lattice with a pore size of 1.2 nm, making it possible to encapsulate small molecules within the nanoporous network. When deposited at 300 K, the molecules retain their superconducting structure and minimize substrate interaction by aligning their long molecular axis perpendicular to the substrate. These results provide guidelines for facile controllable fabrications of epitaxial superconducting and/or magnetic confined condensates on metal surfaces.

1 Introduction Organic superconductors [1] represent a special class of unconventional superconductors, where partial oxidation of organic layers stabilizes superconductivity up to 12 K [2]. Apart from being easily fabricated in high-quality single crystals, organic superconductors have remarkable similarities with their high-Tc counterparts, such as symmetry of pair wave-function, proximity, and/or coexistence of other competing insulating or magnetic orders and anisotropic transport properties [3–6]. Moreover, they can be fabricated as single and multilayers islands, which offer the possibilities to study unconventional superconductivity down to the nanoscale limit.

In our previous work [7], we have shown that superconductivity of $(BETS)_2GaCl_4$ on Ag(111), where BETS = bis(ethylenedithio) tetraselenafulvalene, is robust enough to survive down to the size of a few molecular pairs. The observed anisotropic superconducting gap depends on the size of the molecular chains below 50 nm, with the nodal direction along the inorganic anions [7]. The survival of superconductivity at the nanoscale is not yet understood, since the substrate–molecule interactions are expected to modify the band filling and/or overlap strength of donor molecules and may rather favor insulating ground states [8, 9]. However, the interactions between organic molecules and metal surfaces are rather intricate, as they arise from a variety of bonding mechanisms such as covalent, van der Waals, hydrogen bonds, Pauli repulsion, and charge transfer [10].

In a heteroepitaxial $(BETS)_2GaCl_4$/Ag(111) system, these interactions can be minimized through specific molecular orientation where BETS rings are perpendicular to the substrate, thus frontier orbitals overlap only via proximity of sulfur atomic orbitals [7]. Based on recent DFT calculations [11], it has been shown that BETS molecules are weakly chemisorbed on the surface by partial charge injection from Ag(111), where each BETS molecule receives about 0.22 e. The $GaCl_4^-$ anion receives this charge in addition to

0.2 e directly from each BETS, making a total charge transfer of 0.84 e. In addition to the charge transfer between BETS dimers and Ag(111), the heteroepitaxial process, as in the present study, will also reduce the intradimer separation of $(BETS)_2GaCl_4$ by about 0.3 Å along the stacking directions. Consequently, the substrate effect will not only alter the degree of band filling, but will also modify the overlapping strength of BETS dimers. Qualitatively, the stability of single-layer superconductivity may be attributed to a strong overlap of dimer's molecular orbitals and deviation from quarter band filling (as a result of charge transfer between the Ag(111) and the BETS dimer). However, other issues such as the strength of dimerization and band width are important, therefore theoretical studies are necessary to model the details of substrate interaction and elucidate the stability of nanoscale superconducting properties.

In order to study the effect of dimensionality and finite-size effects [5, 7] and test theories [11–13] on the effect of adsorbate–substrate interactions, the fabrication of a crystalline monolayer with known registry or molecular orientation with respect to the underlying substrate is absolutely necessary. To date, there is no report on the fabrication process of a high-quality crystalline monolayer of $(BETS)_2GaCl_4$ islands. In the current article, we address this issue by controlling the growth process to fabricate monolayer islands of two distinct structural motifs, namely the λ-like (parallel) and triangular nanoporous network of $(BETS)_2GaCl_4$, known as the Kagome lattice. Based on high-resolution STM topographic images, we clearly identify an insulating Kagome network and superconducting λ-like motif as the most stable phases at deposition temperatures of 125 and 300 K, respectively.

2 Experimental

2.1 Synthesis of $(BETS)_2GaCl_4$ single crystal

Single crystals of λ-$(BETS)_2GaCl_4$ have been synthesized by an electrochemical crystallization process in a standard H-type cell under an argon atmosphere that involves oxidation reaction of the BETS donor. The procedures are similar to methods published elsewhere [14, 15].

2.2 Fabrication of monolayer islands on Ag(111) Single crystals of λ-(BETS) 2GaCl4 were resistively heated at 160 °C in UHV conditions. The base pressure during the deposition was below 8×10^{-10} Torr. The process led to the formation of monolayer islands of $(BETS)_2GaCl_4$ that are epitaxially grown over the Ag(111) surface. The growth mode, in both cases, is identified as Volmer–Weber type, where the interaction between the adsorbed molecules is larger than the adsorbate–surface interaction. The substrate temperature is constant during the deposition and is typically set in the range of 100–300 K.

2.3 Imaging the structural and electronic properties All STM measurements are performed with a commercial Joule Thomson scanning tunneling microscope operated at 1 K under ultrahigh vacuum conditions (SPECS Surface Nano Analysis GmbH, Germany). The tungsten STM tip was made by electrochemical etching. High-resolution topographic images were obtained by recording the STM tip height at constant current, while scanning the sample surface. Typical imaging parameters range from 10 mV to 1 V and 30 to 300 pA for the bias voltage and tunneling current, respectively. The scanning tunneling spectroscopy is performed using the standard lock-in technique, with a bias modulation of 1 mV rms. Before interrupting the feedback loop, the junction impedance is stabilized at about 0.1–1 GΩ.

3 Results and discussion

3.1 Growth at low deposition temperature

Figure 1 displays typical examples of various motifs that we have observed in our studies. At low deposition temperatures (110 K) (see Fig. 1a), the donors (BETS) form parallel arrangement, as depicted by the schematic overlays. The blue and yellow lines illustrate the locations of BETS dimers of top and bottom bilayer islands. This is usually referred to as the λ-motif in the literature [14]. Here, BETS dimers are stacked along ⟨110⟩ directions with the long molecular axes parallel to the Ag(111) surface, thus forming chain-like structure where $GaCl_4^-$ molecules reside between the chains. In each dimer, the π–π stacking of BETS monomers is offset vertically from each other by about 50 pm, see the line profile of the single layer in the lower right inset. A high-resolution zoom on a single layer island is shown in the lower left inset. Structural details such as the unit cell, locations of BETS, and $GaCl_4^-$ are clearly visible and schematically illustrated in the overlays.

Due to the lattice symmetry of Ag(111), there are three equivalent orientations for BETS dimers to form chain-like or regular two-dimensional networks. As we raise the deposition temperature to 115 K, we have observed a mix of two stacking orientations, termed as A and B (Fig. 1b). Regular arrangements of molecular units along three stacking orientation were observed at a deposition temperature of 125 K (Fig. 1c and d). Each of the small molecular arrangements of Fig. 1c represents one component in the trimer network of Fig. 1d. Let us discuss the packing of these structures in more detail. The size of the molecular units is about 14.8 and 14.6 Å along ⟨110⟩ and $\langle 11\bar{2}\rangle$ directions, respectively. The perfect stacking of BETS molecules along ⟨110⟩ underlines an epitaxial growth. A model for the packing geometry from the size, shape of molecules and epitaxial consideration is depicted in the overlay. The model shows that BETS dimers are spaced at three times the lattice constant of Ag(111) or roughly 9 Å, whereas $GaCl_4^-$ molecules gap the two dimerized units. Interestingly, the two dimers shift laterally about 0.2 nm along the $\langle 11\bar{2}\rangle$ direction. The inset shows a close-up view on one unit imaged with higher bias parameters of 1 V and 375 pA. Lines in the inset mark the edges of the two dimers.

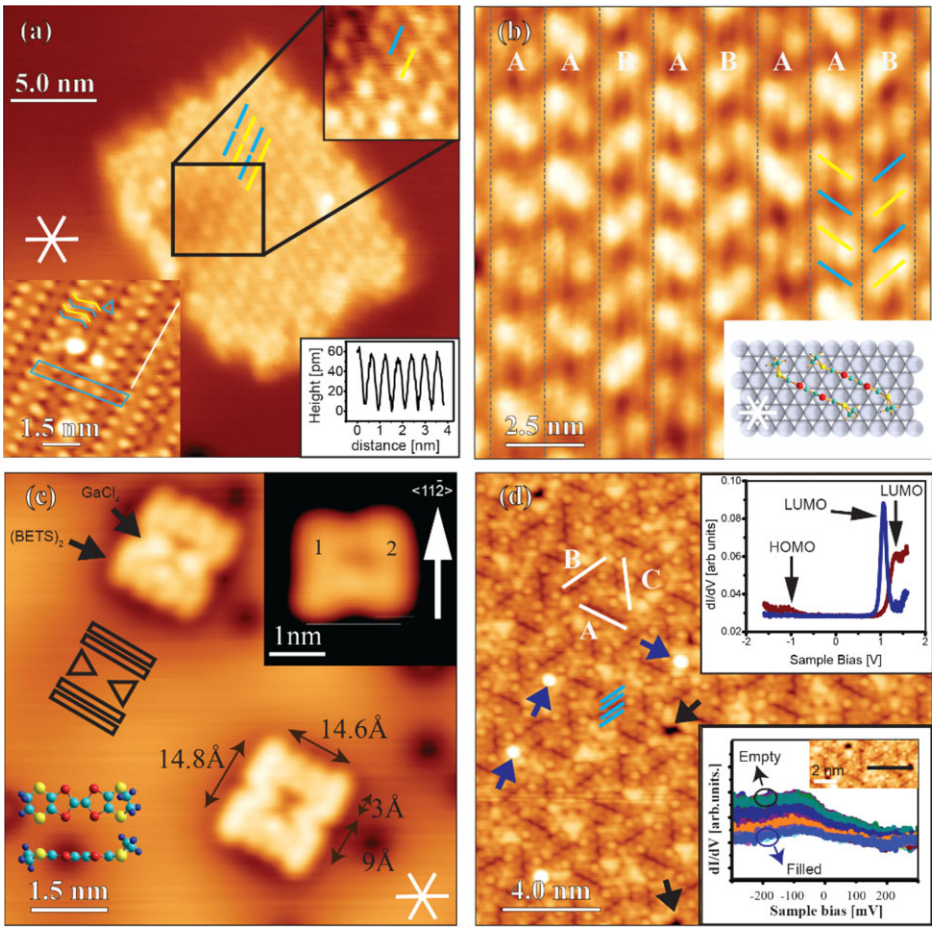

Figure 1 Structural motifs obtained at lower deposition temperatures. (a) STM image of a double layer island on a terrace, deposited at 110 K. The overlays in yellow and blue show top and bottom BETS dimers. The lower left inset is a high-resolution zoom showing parallel or λ-like motif of a single layer island. The location of BETS dimers, $GaIC_4^-$, and the unit cell are depicted in the overlays. The right inset shows the chain profile of island in the lower left inset. (b) At a deposition temperature of 115 K, an irregular herringbone molecular structure is observed. A and B are two different orientations of the chains, as illustrated in the overlays. (c) A close-up view of two unit cells on bare Ag(111) surface, grown at 125 K. Similar to the bulk phase, the unit cell contains four molecules of BETS and two molecules of $GaIC_4^-$. The inset shows a lateral shift of about 0.2 nm between the two dimers. (d) Topographic image of a 25-nm island prepared under the same conditions as in (c) showing a Kagome lattice structure. The slanted lines A, B, and C mark the BETS dimers that are stacked along three symmetric directions of ⟨110⟩. Arrows in black and blue point at empty and occupied sites, respectively. STS measurements at large and small scales are shown in the insets, see text for details. All images were taken at 1 K with the same biasing conditions (150 mV and 100 pA) except the lower inset of (a) was imaged at 150 mV and 230 pA and the inset of (c) was imaged at 1.24 V and 1 nA.

When the smaller molecular units condense to form large islands, they crowd in trimers as shown in Fig. 3d. In a two-dimensional system, this situation leads to orientational frustration of BETS dimers and thereby a Kagome lattice [16] is formed. The slanted lines A, B, and C mark the stacking orientation of a triangular unit along ⟨110⟩ directions. The blue lines mark the locations of two dimers in the triangular unit. The observed Kagome lattice shows vacancies, which can be used to encapsulate guest molecules, such as $GaCl_4^-$. However, orientation-dependent interactions may also lead to high selectivity of guest molecules.

The tolerance of the Kagome lattice to host guest molecules can be illustrated here when considering the physisorption of $GaCl_4^-$. For example, the voids, which are marked by the black arrows in Fig. 1d, can be filled with other diffused or incoming molecules during the deposition process. Since the steric hindrance restricts the incorporation of BETS dimers, the voids can be filled with $GaCl_4^-$ molecules only. As a result, the regular bright spots, as marked by the blue arrows, are due to the $GaCl_4^-$ of the second layer. The scanning tunneling spectroscopy (STS) on occupied site (blue curve) shows only a LUMO state at 1.07 eV, while STS on the dimer site (red curve) shows a HOMO–LUMO gap of 2.37 eV, see upper inset of Fig. 1d. A spatially resolved low bias STS across 4 nm on the island, see lower inset, shows only background from the Ag(111) substrate without any features of molecular states near

Fermi energy. The spatial dependence of the background spectra shows higher intensity on pore sites than on dimers or occupied sites. From these results, we conclude that the Kagome structure of $(BETS)_2GaCl_4$ is insulating, however, the effect of substrate on the gap electronic properties cannot be entirely excluded.

3.2 High-resolution imaging of $BETS_2GaCl_4$

Next we address high-resolution STM imaging of organic molecules by tip functionalization, which occurs spontaneously during imaging. As the standard STM imaging technique is only sensitive to local variation of the density of states near Fermi level, topographic images of organic molecules contain no structural details of submolecular features. However, with proper tip functionalization, several groups [17–19] have been able to obtain high-resolution images on organic molecules with STM or AFM. Here, we demonstrate a similar imaging method to reveal the chemical contrast on charge-transfer complexes by utilizing the electron affinity of the acceptor molecule to sense the spatial variation in charge density of donor molecules. The method utilizes the physisorbed molecules that can be trapped between the STM tip and surface at low bias voltage (below 50 mV) and relatively high current (above 1 nA). The trapping occurs when the STM tip encounters a loosely bound molecule on the island. The identity of the molecule is not clear yet, but it could most likely be either CO or $GaCl_4^-$, as these are the only physisorbed molecules that STM tip encounters while scanning the porous network. By keeping the tunneling current above 1 nA and the bias voltage below 50 mV, higher-resolution images of $(BETS)_2GaCl_4$ were obtained. The details of the manipulation process will be published elsewhere.

Figure 2a shows the quality of the STM image resolution before (upper half) and after tip functionalization (lower half). Every BETS molecule within the dimerized units is clearly resolved as a stripe containing two or three bright spots for an inner or outer molecule, respectively. The BETS donor molecules are forming dimers with $GaCl_4^-$ molecules located at the periphery. With BETS rings perpendicular to the surface, dimers are segregated in units of two facing each other with a lateral shift of 0.3 nm along the $\langle 11\bar{2} \rangle$ packing direction of the Ag lattice. The edges of inner BETS molecules are bent outwards, while the outer BETS molecules are almost planar. In earlier studies, it has been shown that charge transfer induces structural modifications of molecules and alters the alignment of the energy levels with the metal interface [20, 21]. The structural variation within the dimers observed here is in sharp contrast with the bulk structure and confirms the earlier claim [22] of charge disproportionation in the BETS dimers. It also indicates that the inner BETS molecule is predominantly participating in the charge-transfer process, while the outer BETS molecule delocalizes the charge through overlapping with neighboring dimers. Moreover, the image of the inner BETS shows more details on the submolecular contrast than the outer BETS (Fig. 2b), which indicates a difference in the electronic characters between

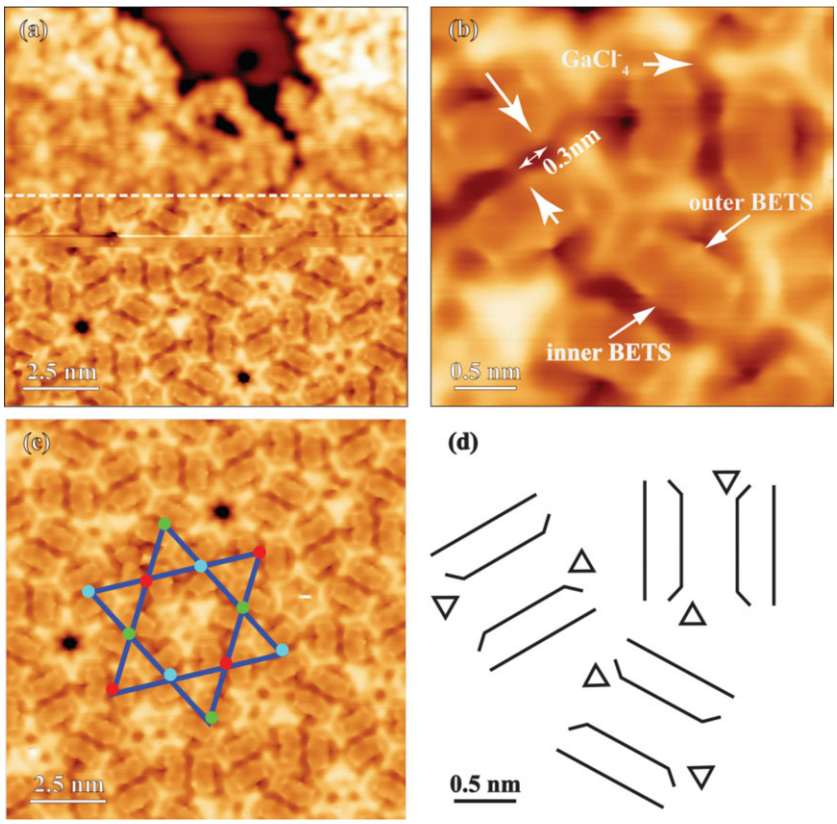

Figure 2 Kagome lattice of BETS on Ag-(111). (a) Topographic image of $(BETS)_2$-$GaCl_4$ monolayer near Ag(111) interfacial region before (top of dotted line) and after (bottom of dotted line) spontaneous tip functionalization. (b) A higher-resolution image, showing details of molecular packing, such as the lateral shift and differences in backbone structures between inner and outer BETS molecules within each dimer. (c) The unit cell of the Kagome lattice. The lattice points with colors of cyan, red, and green represent the three different orientations of BETS long molecular axis on Ag (111). The model structure in (d) illustrates molecular packing of the trimer in (b). The imaging parameters are 50 mV and 1 nA for bias voltage and tunneling current, respectively.

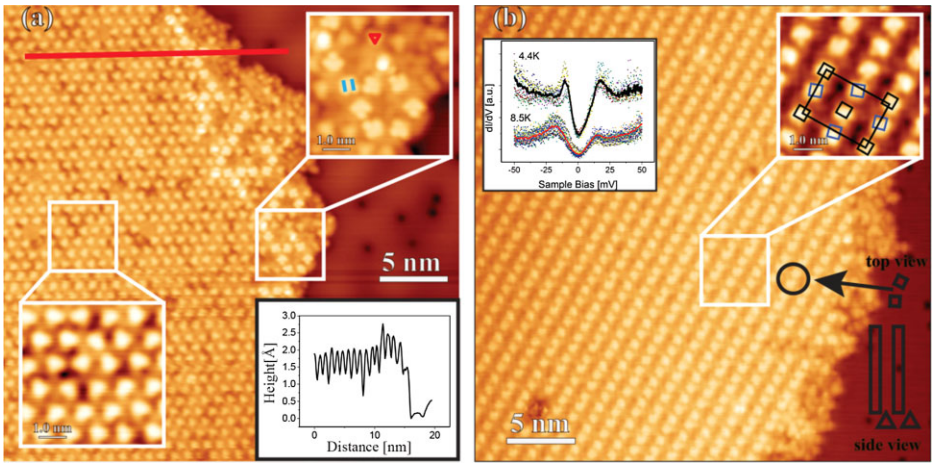

Figure 3 Growth of $(BETS)_2GaCl_4$ on Ag(111) at 300 K. (a) STM image of $GaCl_4^-$ terminated island. The top right inset is a close-up view, showing the molecular packing of BETS dimers (blue lines) and $GaCl_4^-$ (red triangle) near the edge of a sub-two-layer island. The left inset is a close-up view of $GaCl_4^-$ packing. The height profile along line in red is shown in the lower right inset. (b) STM image of an island terminated with BETS layer, showing dimers with alternating orientation. The right inset shows a close-up view with overlay depicting the molecular orientation and a rectangular unit cell of dimensions $1.74 \times 2.67\,nm^2$. The tunneling spectroscopy at 4.4 K, top left inset, shows a V-shape superconducting gap with coherence peaks at ± 12 mV. The coherence peaks broaden when the temperature is increased from 4.4 to 8.5 K. The imaging parameters are 150 mV and 100 pA for bias voltage and tunneling current, respectively.

the molecules and may be attributed to the partially filled bands of the inner BETS molecules. Again, the dimers are grouped as units of two that alternate regularly along equivalent ⟨110⟩ packing directions forming a Kagome lattice with a unit cell of ten BETS dimers and ten $GaCl_4^-$ molecules, i.e., quintuple the number of molecules contained in the unit cell of the λ-motif. Fig. 2(c) shows high-resolution image of the Kagome lattice with an overlay depicting the unit cell. The three colors; cyan, red, and green of the lattice points represent the three possible orientations of BETS dimers in the Kagome network that are perfectly aligned with the ⟨110⟩ directions.

3.3 Growth at room temperature Finally, we address the growth of $(BETS)_2GaCl_4$ on Ag(111), when the substrate temperature is raised to 300 K. Two distinctive features of room-temperature growth are observed: first, the molecules tend to favor vertical growth with no sign of nucleation at the top of step edge; instead nucleation starts at the step-edge bottom. Secondly, the unit cell is still similar to the λ-motif of the bulk structure with the molecular orientation totally governed by the epitaxial process, along the ⟨110⟩ direction, rather than the step-edge orientation. Figure 3 illustrates two examples of different layer terminations: $GaCl_4^-$ in Fig. 3a and BETS cations in Fig. 3b. A structural model of vertical growth is depicted in Fig. 3b showing top and side views of BETS molecular packing. The $GaCl_4^-$ anions layer, Fig. 3a, are densely packed in a hexagonal pattern with a lattice constant of 1 nm. BETS cations are located beneath the $GaCl_4^-$ layer. A few molecules of the BETS layer are forming regular aggregates at the edge of the island. The overlays shown in the top right inset illustrate the molecular packing of both BETS and $GaCl_4^-$. Here, the BETS dimers are aligned with their long molecular axis perpendicular to the surface and therefore appear as squares, whereas $GaCl_4^-$ appear as triangular spots just like the rest of the island.

The nucleation of the molecular crystal at the step edge bottom is not surprising and has been reported in many organics on metal surfaces [23]. In this case, the molecules do not have enough energy to cross the step edge and have only one possibility to diffuse on lower terrace of the step and form crystalline islands. What is unusual here is that the cation molecules are oriented with their long molecular axis perpendicular to the Ag surface. This situation may be triggered by the initial hexagonal packing of the anion layer on Ag(111). Due to depopulation of surface state electrons and enhanced diffusion at 300 K, the anions maximize their interactions by crowding in an hexagonal arrangement to stabilize the island structure. After the anion layer is formed, incoming BETS dimer cations will have to also pack densely for a charge-transfer ratio of 2 to 1 to occur. The only possibility for this to occur is vertical alignment of BETS molecules on Ag(111) surface, see Fig. 3b. We conjecture that such a scenario explains the reasons for the vertical alignments. The full description of bonding and the kinetics of the interaction process versus temperature require heavy quantum-mechanical calculations, which is beyond the scope of this work.

The scanning tunneling spectroscopy on the island shows a "V"-shaped superconducting gap around the Fermi level with coherence peaks around 12 meV. The top left inset of Fig. 3b shows the STS measurement taken at two different temperatures. As the temperature is increased from 4.4 to 8.5 K, the coherence peaks are broadening. It is worth pointing out that the broadening is clearly visible near the

bulk transition temperature of 8.5 K but the gap still maintains its characteristics. This suggests that the transition temperature of a single layer may be slightly higher than the bulk value. The full evolution of superconducting to metallic phase will be carried out in future studies. The unconventional energy gap is large compared to a similar T_c value of conventional superconductors, however, this is a characteristic signature of many organic superconductors. The coherence peaks are asymmetric with a similar width to our earlier studies [7]. The large width of coherence peaks can be attributed to substrate–molecules interactions which tend to limit the lifetime of quasiparticles. It is remarkable that the superconducting condensate of a single monolayer island survived interaction effects of the metal surface. Further theoretical investigation would be very helpful to provide insight into the details of interaction effects.

4 Conclusions In summary, the epitaxial growth of organic insulating or superconducting monolayer islands on Ag(111) has been achieved at various growth temperatures. The substrate temperature during the growth process has the major effect on both nucleation and size of the unit cell. Within the temperature range of 100–120 K, the nucleation starts primarily on top of step edges. Above 125 K, the BETS dimers start to alternate regularly along the three equivalent orientations of $\langle 110 \rangle$ packing directions, forming a Kagome lattice with a triangular nanoporous network. With a pore size of $\sim$1.2 nm, it is possible to accommodate magnetic or nonmagnetic molecules, which are highly suitable for tailoring the ground-state properties of single-layer organic charge transfer complexes. Finally, superconducting islands are fabricated when deposition is carried out at room temperature. A robust superconducting d-wave gap is ubiquitously observed with broadened coherence peaks due to molecules–substrate interactions. The preferential condensation of molecules into insulating or superconducting monolayers versus substrate temperature provides a unique key control to pattern nanoscale superconducting islands in the future.

Acknowledgements The authors acknowledge R. Rankin and J. Greeley of Purdue University for generously sharing the results of their DFT data, H. Kobayashi of Nihon University, S. Hla of Ohio University, Y. Tanaka of Nagoya University for fruitful discussions. We acknowledge the funding from the Slovenian Research Agency (ARRS) under Program No. P1-0099 and the MP1201 COST-action project.

References

[1] D. Jérome, A. Mazaud, M. Ribault, and K. Bechgaard, J. Phys. (France) Lett. **41**, 95 (1980).
[2] A. M. Kini, U. Geiser, H. H. Wang, K. D. Carlson, J. M. Williams, W. K. Kwok, K. G. Vandervoort, J. E. Thompson, and D. L. Stupka, Inorg. Chem. **29**, 2555 (1990).
[3] T. Ishiguro, K. Yamaji, and G. Saito, Organic Superconductors, 2nd edn. (Springer-Verlag, Heidelberg, 1998), p. 125.
[4] S. Uji, H. Shinagawa, T. Terashima, T. Yakabe, Y. Terai, M. Tokumoto, A. Kobayashi, H. Tanaka, and H. Kobayashi, Nature **410**, 908 (2001).
[5] J. Brooks, in: Handbook of High Temperature Superconductivity, edited by J. R. Schrieffer and J. S. Brooks (Springer, New York, 2007).
[6] N. Doiron-Leyraud, P. Auban-Senzier, S. R. de Cotret, C. Bourbonnais, D. Jérome, K. Bechgaard, and L. Taillefer, Phys. Rev. B **80**, 214531 (2009).
[7] K. Clark, A. Hassanien, S. Khan, K.-F. Braun, H. Tanaka, and S.-W. Hla, Nature Nanotechnol. **5**, 261 (2010).
[8] H. Seo, C. Hotta, and H. Fukuyama, Chem. Rev. **104**, 5005 (2004).
[9] T. Mori, Chem. Rev. **104**, 4947 (2004).
[10] A. Tkatchenko, L. Romaner, O. T. Hofmann, E. Zojer, C. Ambrosch-Draxl, and M. Scheffler, MRS Bull. **35**, 435 (2010).
[11] R. Rankin and J. Greeley, unpublished results.
[12] W. Liu, A. Tkatchenko, and M. Scheffler, Acc. Chem. Res. **47**, 3369 (2014).
[13] V. G. Ruiz, W. Liu, E. Zojer, M. Scheffler, and A. Tkatchenko, Phys. Rev. Lett. **108**, 146103 (2012).
[14] A. Kobayashi, T. Udagawa, H. Tomita, T. Naito, and H. Kobayashi, Chem. Lett. **12**, 2179 (1993).
[15] H. Kobayashi, H. Cui, and A. Kobayashi, Chem. Rev. **104**, 5265 (2004).
[16] I. Syôzi, Prog. Theor. Phys **6**, 306 (1951).
[17] L. Gross, N. Moll, F. Mohn, A. Curioni, G. Meyer, F. Hanke, and M. Persson, Phys. Rev. Lett. **107**, 086101 (2011).
[18] L. Gross, F. Mohn, N. Moll, P. Liljeroth, and G. Meyer, Science **325**, 1110 (2009).
[19] R. Temirov, S. Soubatch, O. Neucheva, A. Lassise, and F. Tautz, New J. Phys. **10**, 053012 (2008).
[20] S. Bedwani, D. Wegner, M. F. Crommie, and A. Rochefort, Phys. Rev. Lett. **101**, 216105 (2008).
[21] T.-C. Tseng, C. Urban, Y. Wang, R. Otero, S. L. Tait, M. Alcamí, D. Écija, M. Trelka, J. M. Gallego, and N. Lin, Nature Chem. **2**, 374 (2010).
[22] K.-i. Hiraki, M. Kitahara, T. Takahashi, H. Mayaffre, M. Horvatić, C. Berthier, S. Uji, H. Tanaka, B. Zhou, and A. Kobayashi, J. Phys. Soc. Jpn. **79**, 074711 (2010).
[23] S. M. Barlow and R. Raval, Surf. Sci. Rep. **50**, 201 (2003).